# On the modelling of the friction characteristics of railway vehicle brakes

Marc Ehret, Ernst Hohmann and Andreas Heckmann

The rules and standards that define the requirements and methods for the layout of friction brake systems for railway vehicles still demand extensive experimental surveys since the general confidence in the theoretical predictability of the brake pad friction behaviour is limited. In fact, a review of numerous measurements from dynamometer test rigs exposes a large variation of the friction characteristics. Nevertheless, these measurements could be exploited to develop an elaborate friction modelling approach that includes deterministic and stochastic influences. The comparison of vehicle measurements from field tests with simulation results reveals that a significant improvement of the theoretical predictability of braking distances is within reach. Consequently, this applies as well for a more virtual layout and acceptance procedure for railway vehicle brake systems in the future.

# Taylor & Francis Word Template for journal articles

Marc Ehret [a]*, Ernst Hohmann[b] and Andreas Heckmann[a]

[a]*German Aerospace Center (DLR), Institute of System Dynamics and Control, Oberpfaffenhofen, Germany;* [b]*Knorr Bremse Rail Vehicle Systems, Munich, Germany*

marc.ehret@dlr.de for the *corresponding author (ORCID-ID 0000-0001-5027-3865)

Provide short biographical notes on all contributors here if the journal requires them.

# On the modelling of the friction characteristics of railway vehicle brakes

The rules and standards that define the requirements and methods for the layout of friction brake systems for railway vehicles still demand extensive experimental surveys, since the general confidence in the theoretical predictability of the brake pad friction behaviour is limited. In fact, a review of numerous measurements from dynamometer test rigs expose a large variation of the friction characteristics. Nevertheless, these measurements could be exploited to develop an elaborate friction modelling approach that includes deterministic and stochastic influences. The comparison of vehicle measurements from field tests with simulation results reveal that a significant improvement of the theoretical predictability of braking distances is within reach. Consequently, this applies as well for a more virtual layout and acceptance procedure for railway vehicle brake systems in the future.

Keywords: friction models, railway brakes, braking distance

## 1 Motivation and Objectives

Due to the rail-bound traffic there is a strong correlation of safety and throughput with the braking deceleration in emergency cases of railway vehicles. The requirements for the brake system layout of passenger trains are specified by the TSI-Loc&Pas [1], see Sec. 4.2.4. The TSI refers to EN-14531-1/2 [2, 3], where methods and algorithms for calculating and verifying the conformity with these requirements are defined. These standards emphasize the large influence of the coefficient of friction (COF) of the brake pad on the braking distance calculation, demand experimental proofs and appropriate averaging at least with respect to different speed ranges. Figure 1 exemplifies the underlying problem: the measured decelerations significantly differ as a function of the initial train velocity, even if the identical brake pressure is applied.

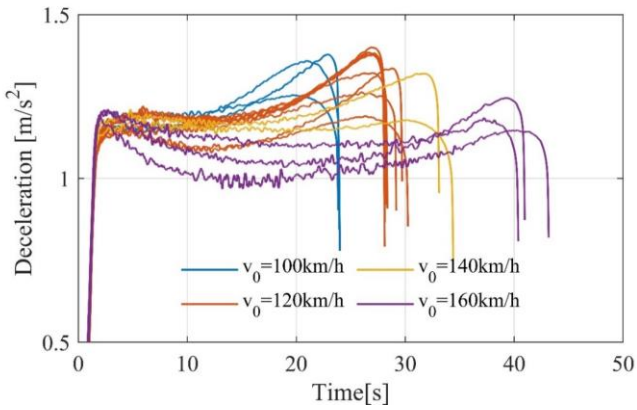


Figure 1: Comparison of measured instantaneous deceleration of a train during friction brake applications for different initial velocities

An additional annotation in to EN-14531-1 nominates several quantities that rule the brake pad friction behavior under transient conditions, but regrets the lack of knowledge with regard to quantitative details. This is why the standard demands experiments instead, in order to predict the brake performance of each specific vehicle type. This process proved to be appropriate in the past, although it is prone to changes and unexpected conditions not covered by the underlying tests. And of course, the process is elaborate, time-consuming and expensive. The use of mathematical models for the estimation of instantaneous and load case dependent brake forces of railway disc brakes is discussed in [4, 5]. However, the presented models are deterministic and do not consider the stochastic nature of friction forces.

It is the above-mentioned lack of knowledge and predictability of friction behavior that motivates the present paper. The objective is to gain and validate simulation models, that allow to predict the brake performance of a specific railway vehicle type, i.e. its nominal braking distances, and quantify its uncertainty, i.e. the braking distance distributions, that comes with stochastic influences. On the long run, the authors aim to pave the way to a more virtual layout and acceptance procedure for the design of railway vehicle brake systems.

The contribution of this work has the following structure: In Sec. 2 the authors introduce a large number of brake process measurements recorded on a dynamometer test rig in order to review the brake pad friction characteristics under transient conditions. Sec. 3 presents simulation models, which are used in Sec. 4 to identify the deterministic influences on the friction behavior based on the measurements from the test rig. Sec. 5 is dedicated to the stochastic impact on the brake pad friction. Sec. 6 transfers the gained knowledge from dynamometer test rigs to fields tests and Sec.7 concludes the paper.

## 2 Analysis of a single brake disc unit using dynamometer tests

The following review of the brake pad friction characteristics is based on tests conducted on a full scale dynamometer test rig of Knorr Bremse SfS in Munich that complies with the requirements given in EN-14531 [2, 3] and EN-15328 [6], respectively. The principle design of the test rig and the acting forces are drawn in Figure 2. The disc brake or wheel-disc brake is mounted on an axle and connected to the inertia dynamometer. The dynamometer simulates an adjustable rotating inertia $m_{eff}$ representing the dynamic mass that is decelerated by a single disc brake unit. The caliper unit is actuated by the brake cylinder pressure $p_C$ in order to apply the normal force $F_N$ on each side of the disc. According to [2], the *total clamp force* $F_C$ represents

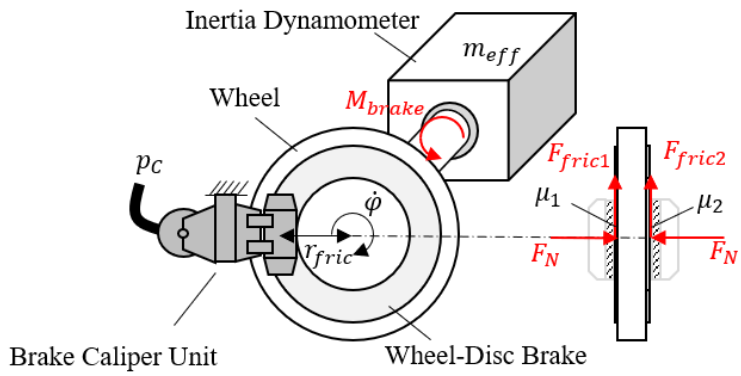


Figure 2: Sketch of the dynamometer test rig applied for a wheel-disc brake [4]

the sum of normal forces acting in all contacts of a disc brake unit arrangement, yielding $F_C = 2 \cdot F_N$. The brake torque $M_{brake}$ caused by the friction forces $\left(F_{fric1} + F_{fric2}\right)$ applied at the radius $r_{fric}$ is measured together with the rotational velocity $\dot{\varphi}$. Assuming $\mu_1 \approx \mu_2 \approx \mu$, the instantaneous COF $\mu(t)$ then follows from

$$\mu(t) = \frac{M_{brake}(t)}{2 \cdot r_{fric} \cdot F_N(t)} = \frac{M_{brake}(t)}{r_{fric} \cdot F_C(t)}. \quad (1)$$

Table 1 summarizes the experiments to be further discussed. 12 different load cases with 5 different specimen of an organic brake pad sum up to 1950 brake stop brake applications. During each brake process the inertia is decelerated from the initial vehicle velocity $v_0$ and $\dot{\varphi}_0$, respectively, until standstill by applying a constant brake pressure, i.e. clamp force. The experimental conditions and the sequence were identical for each specimen yielding at least 18 brake processes per specimen and load case.

Table 1: Initial Velocity $v_0$, effective mass $m_{eff}$, clamp force $F_C$ and number of single brake applications of each pad specimen tested on full scale dynamometer test rig

| Load case | $v_0$ [km/h] | $m_{eff}$ [kg] | $F_C$ [kN] | Number of single brake applications per pad specimen | | | | | |
|---|---|---|---|---|---|---|---|---|---|
| | | | | specimen 1 | specimen 2 | specimen 3 | specimen 4 | specimen 5 | all |
| V0100_Case1 | 100 | 7250 | 33 | 40 | 20 | 40 | 40 | 40 | 180 |
| V0100_Case2 | 100 | 8250 | 38 | 40 | 20 | 40 | 40 | 20 | 160 |
| V0100_Case3 | 100 | 9050 | 44 | 40 | 20 | 40 | 39 | 20 | 159 |
| V0120_Case1 | 120 | 7250 | 33 | 40 | 20 | 40 | 40 | 40 | 180 |
| V0120_Case2 | 120 | 8250 | 38 | 40 | 20 | 40 | 40 | 20 | 160 |
| V0120_Case3 | 120 | 9050 | 44 | 40 | 20 | 40 | 40 | 20 | 160 |
| V0140_Case1 | 140 | 7250 | 33 | 36 | 18 | 36 | 36 | 37 | 163 |
| V0140_Case2 | 140 | 8250 | 38 | 36 | 18 | 36 | 36 | 18 | 144 |
| V0140_Case3 | 140 | 9050 | 44 | 36 | 18 | 36 | 36 | 18 | 144 |
| V0160_Case1 | 160 | 7250 | 33 | 40 | 20 | 40 | 40 | 40 | 180 |
| V0160_Case2 | 160 | 8250 | 38 | 40 | 20 | 40 | 40 | 20 | 160 |
| V0160_Case3 | 160 | 9050 | 44 | 40 | 20 | 40 | 40 | 20 | 160 |
| All load cases and specimen | | | | | | | | | 1950 |

A scaled representation of the transient friction measurements corresponding to the $n$=163 brake processes of load case V0140_Case1 is displayed in Figure 3. In detail, each light gray curve presents $\mu_i(t)$ of a single brake process $i$ and the connection of the mean values at each time instant constitute the bold mean value curve $\bar{\mu}(t)$ in black.

The two medium black curves limit the range of three times the empiric standard deviation $\sigma_\mu(t)$, i.e.

$$\bar{\mu}(t) = \frac{1}{n}\sum_i \mu_i(t)\ , \qquad \sigma_\mu^2(t) = \frac{1}{n-1}\sum_i (\mu_i(t) - \bar{\mu}(t))^2\ , \qquad i = 1, \cdots, n\ . \quad (2)$$

In what follows, the mean value curve $\bar{\mu}(t)$ will be interpreted to be associated to deterministic influences on the brake process, while deviations from this mean value curve are assumed to stem mainly from the stochastic characteristics of the friction process.

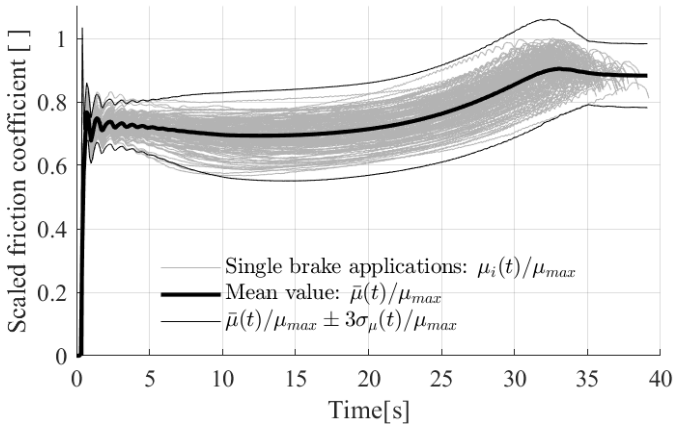


Figure 3: Scaled representation of instantaneous COF of all 163 single brake applications, instantaneous mean value and empirical standard deviation over time for load case V0140_Case1

By averaging the coefficient of friction over the braking distance a friction curve of a brake process is transformed into a single value $\mu_{s,i}$, which may be applied for braking distance calculations according to EN-14531:

$$\mu_{s,i} = \frac{1}{s_{2,i}}\int_0^{s_{2,i}} \mu_i(s)ds\ , \quad (3)$$

$s_{2,i}$ denotes the stopping distance of the brake process starting when 95% of the nominal clamp force is reached. Analogue to Equation *(2)* the mean values $\bar{\mu}_s$ and standard

deviation $\sigma_{\mu_s}$ are calculated for each specimen and load case. The results normed by the observed maximum value $\mu_{max}$ are compared in Figure 4. The upper plot clearly demonstrates that $\bar{\mu}_s$ is decreasing with increasing initial velocity regardless of the specimen. The values of $\bar{\mu}_s$ for load cases with 100km/h are about 16% larger compared to those with 160 km/h related to $\mu_{max}$. In comparison, the relative difference of $\bar{\mu}_s$ between the specimen is smaller 4 % for single load cases. If $\bar{\mu}_s$ is calculated over all load cases, the relative difference of the specimen is 2%. Figure 4 additionally presents an impression on the deviations of the variance originating from different pad samples. A trend to higher standard deviations for higher initial velocities is observed for all specimen. For a single disc brake this deviation leads to a standard deviation of the resulting braking distance $1\sigma_s \approx 2\%$ for 100 km/h and $1\sigma_s \approx 5\%$ for 160 km/h. By

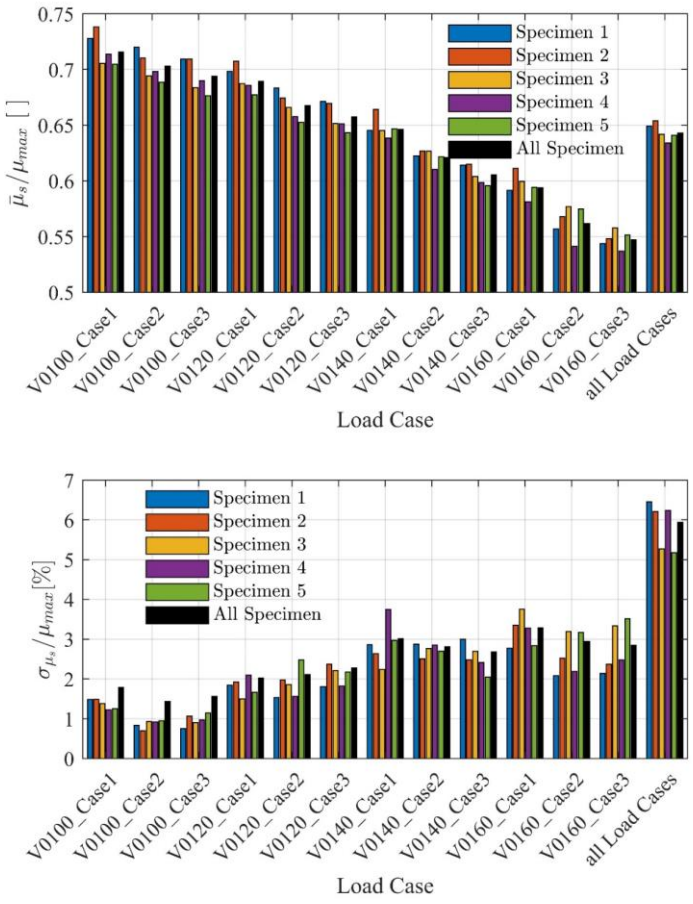


Figure 4: Overview on mean values of the 15 load cases, each averaged with respect to the braking distance (above) and the associated standard deviations (below)

comparing the pillars of $\sigma_s$ for *all Load Cases* with those of the single load cases, it becomes apparent that the consideration of a single averaged COF representing all load cases is doubling or even tripling the standard deviation due to the systematic differences between the single load cases.

As mentioned in EN-14531 and discussed in [7], [5] and [4], it is assumed that surface disc and pad temperatures have an influence on the friction characteristics caused by thermomechanical processes acting in the frictional boundary layer and vice versa [8]. To take account of this mutual influence, temperature measurements are conducted according to UIC Code 548 [9]. Therefore, the brake disc on the test rig is equipped with six thermoelements, as shown in Figure 5. Each thermoelement is drilled 1mm beneath the friction surface of the disc. The wiring is conducted along the inner ventilation surface and the data is telemetrically transmitted from the rotating shaft to the stator. $T_{fric}(t)$ represents the instantaneous average of these six measurements. It is plotted for load case V0140_Case1 in Figure 6 using the same concept for statistical analysis and presentation as in Figure 3. Although $T_{fric}(t)$ is already the mean value of six sensor signals, a variance of the single brake applications is clearly visible. It is found that the underlying variation of the surface temperature of the single

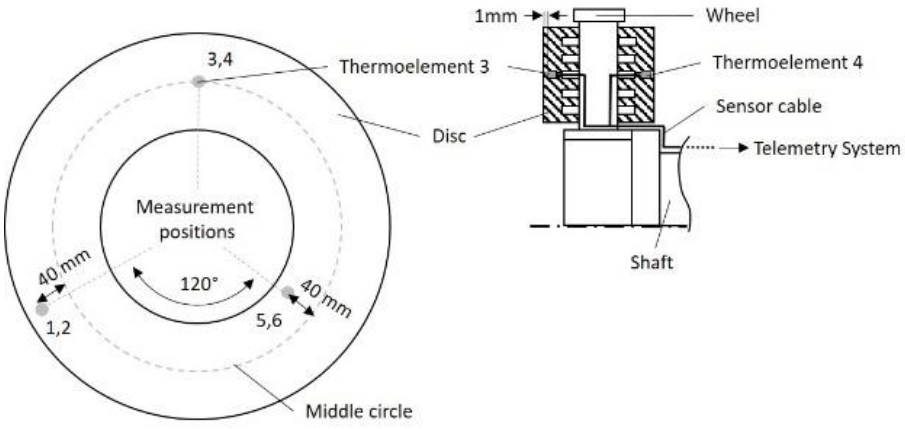


Figure 5: Six measurements positions of the thermoelements placed close to the friction surface (three sensors on each side)

measurement points is strongly influenced by the radial position of the sensor. This could be explained by the development of heat bands and spots on the disc surface during the brake process, as observed in [10, 11].

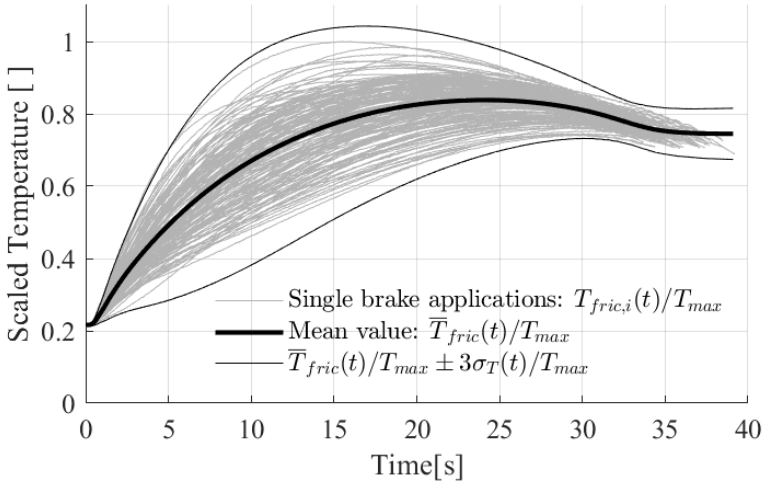


Figure 6: Scaled representation of instantaneous averaged surface disc temperature of all 163 single brake applications, instantaneous mean value and empirical standard deviation over time for load case V0140_Case 1

## 3 Development of a dynamometer model

### *3.1 Friction model*

The friction model to be adopted for the elaboration of the above measurements is based on a dynamic friction model proposed by Ostermeyer [7] for automotive applications and adapted for railway brakes in [4]. The model actually describes the time derivative of the COF $\dot{\mu}(t)$ , which depends on the clamp forces $F_C(t)$, the friction velocity $v_{fric}(t)$ and the averaged disc surface temperature $T_{fric}(t)$ [4]:

$$\dot{\mu}(t) = -\mathrm{a} \cdot \left(\frac{\mu \cdot F_C \cdot v_{fric}}{\mathrm{P_{ref}}}\right)^{\mathrm{x}} - \mathrm{b} \cdot \mu^{\mathrm{y}} - \mathrm{c} \cdot \left(\mu_i \cdot \frac{T_{fric}}{\mathrm{T_{ref}}}\right)^{\mathrm{z}} + \mathrm{d} \cdot \left(\frac{F_C}{\mathrm{F_{ref}}}\right)^{\mathrm{r}}. \qquad (4)$$

The coefficients $\mathrm{a}, \mathrm{b}, \mathrm{c}, \mathrm{d}$ as well as the exponents $\mathrm{x}, \mathrm{y}, \mathrm{z}, \mathrm{r}$ are the quantities to be identified using the measurements from Sec. 2. $P_{ref}, T_{ref}$ and $F_{ref}$ are used for normalization. This model turned out to be well suited as a component model for

vehicle train set simulations with many brake discs. A detailed description of the model and the discussion of other approaches for the simulation of the COF between disc and pad, or wheel and tread, respectively, can be found in [4] and [12].

### *3.2 Temperature model*

A large amount of analytical and numerical approaches exists to calculate the temperatures of automotive and railway brake components depending on different brake scenarios, such as single stop, repeated and continued braking, as shown in [8, 13, 14]. Within this work, the temperature model shall predict the average temperature $T_{fric}(t)$ acting in the disc surface during single stops, which is measured by the six temperature sensors, as described in section 2. The model is supposed to be computationally efficient so that it can be applied to a large number of simulations for single discs and entire trains. Therefore, a one-dimensional model based on two lumped thermal capacities, as shown in Figure 7, is proposed. It includes convection acting at the disc surface and ventilation at the inner cooling fins as well as thermal conductivity between the friction zone and the bulk disc. The influence of the pad and the resulting thermal partitioning is neglected.

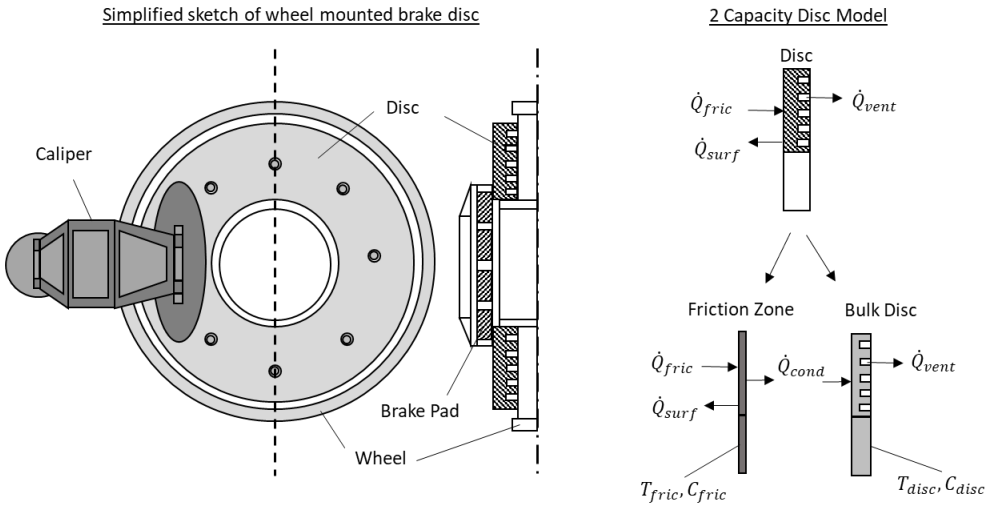


Figure 7: Simplified sketch of wheel mounted brake disc and derivation of a thermal disc model based on two capacities

The thermal model of the brake disc uses the thermal capacity $\mathrm{C_{fric}}$ with the temperature at the friction surface $T_{fric}$ and a lumped disc capacity $\mathrm{C_{disc}}$ with $T_{disc}$ leading to the following two differential equations:

$$\dot{Q}_{fric} - \dot{Q}_{surf} - \dot{Q}_{cond} = \mathrm{C_{fric}} \cdot \dot{T}_{fric}\,, \qquad \dot{Q}_{cond} - \dot{Q}_{vent} = \mathrm{C_{disc}} \cdot \dot{T}_{disc}\,. \tag{5}$$

The heat source term follows from the friction process

$$\dot{Q}_{fric} = \frac{1}{2} \cdot \mu(t) \cdot F_C(t) \cdot v_{fric}\,(t), \tag{6}$$

while the heat conduction between friction zone and bulk disc is driven by the temperature gradient between the capacities and the thermal conductance *G*:

$$\dot{Q}_{cond} = G(T) \cdot \left(T_{fric} - T_{disc}\right). \tag{7}$$

In general, the thermal conductance $[\frac{\mathrm{W}}{\mathrm{K}}]$ is a temperature dependent property. To take account for this dependency, the function $G(T)$ is approximated by the first two terms of a Taylor Series, which is developed at the reference point $(\mathrm{T_{ref}}, \mathrm{G_{ref}})$:

$$G(T_m) \approx \mathrm{G_{ref}} + \frac{\partial \mathrm{G}}{\partial \mathrm{T}_m} \cdot (T_m - \mathrm{T_{ref}}), \quad T_m = \frac{T_{fric} + T_{disc}}{2} \tag{8}$$

$T_m$ is the actual temperature of the conduction zone and assumed to be the mean temperature of bulk disc and friction zone. $\mathrm{G_{ref}}$ represents the value of the conductance at the reference temperature $T_m = \mathrm{T_{ref}} = 273.15\mathrm{K}$ and $\frac{\partial \mathrm{G}}{\partial \mathrm{T}_m}$ is first derivative of the conductance with respect to the temperature, i.e. the slope of $G(T_m)$ at the reference point.

Cooling by convection occurs at the friction surface ($\mathrm{A_{surf}}$) and at the ventilation surface ($\mathrm{A_{vent}}$) and is defined as follows:

$$\dot{Q}_{surf} = h_{surf} \cdot \mathrm{A_{surf}} \cdot \left(T_{fric} - T_\infty\right), \qquad \dot{Q}_{vent} = h_{vent} \cdot \mathrm{A_{vent}} \cdot (T_{disc} - T_\infty). \tag{9}$$

$T_\infty$ denotes the ambient temperature. In this work an exponential approach is proposed to estimate the heat transfer coefficients $h_{surf/vent}$ depended on the velocity of the airflow, which is proportional to the friction velocity $v_{fric}$:

$$h_{surf/vent}(v_{fric}) = \mathrm{h_0} + (\mathrm{h_{ref}} - \mathrm{h_0}) \cdot \left(\frac{v_{fric}}{\mathrm{v_{ref}}}\right)^{\mathrm{ex}}, \tag{10}$$

For $0 < \mathrm{ex} < 1$ the function describes a degressive rise of $h$ with increasing rotational speed, which intersects the points $\mathrm{h_0} = h(0)$ and $\mathrm{h_{ref}} = h(\mathrm{v_{ref}})$. As shown in [15], these curves represent a typical progression assumed for $h(v)$. In conclusion, 10 parameters need to be determined to identify the temperature model $\mathrm{C_{fric}}, \mathrm{C_{disc}}, \mathrm{G_{ref,}} \frac{\partial \mathrm{G}}{\partial \mathrm{T}_m}$ and $\mathrm{h_0}, \mathrm{h_{ref}}$ and ex for both convective heat flows.

### *3.3 Mechanics model*

The mechanics model simulates the deceleration of the rotating disc resulting from the applied instantaneous brake torque $M_{brake}(t)$:

$$M_{brake}(t) = F_C(t) \cdot \mu(t) \cdot \mathrm{r_{fric}} \tag{11}$$

The integration of the deceleration yields the vehicle speed $v(t)$ based on the wheel radius $\mathrm{r_{wheel}}$ and the friction velocity $v_{fric}(t)$, respectively:

$$v(t) = \mathrm{v_0} - \int \frac{M_{brake}(t)}{\mathrm{m_{eff}} \cdot \mathrm{r_{wheel}}} dt, \qquad v_{fric}(t) = v(t) \cdot \frac{\mathrm{r_{fric}}}{\mathrm{r_{wheel}}} \tag{12}$$

### *3.4 Dynamometer model*

Figure 8 presents an overview how the above described friction, temperature and mechanics models interact to simulate the brake processes on the dynamometer test rig. The instantaneous clamp force $F_C(t)$ is the input for all three models. By applying numerical simulation $\mu(t)$, $v(t)$, $T_{fric}(t)$ and $T_{disc}(t)$ are calculated based on

Equations (4)-(12) and the start values $\mu_0$, $v_0$ and $T_0$.

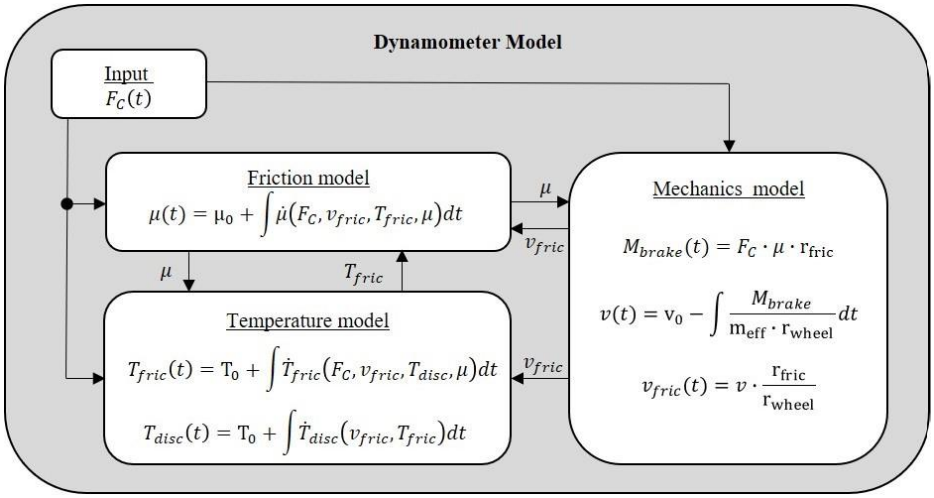


Figure 8: Model to simulate brake applications on dynamometer test rig based on numerical simulation. The eqution of the integrals of the temperature and friction models are given in equations (4) - (10)

## 4 Deterministic model identification

The identification of the model parameters is based on the measurement data presented in Section 2. First, the models are tuned to map the deterministic behaviour, which is assumed to be described by the mean value curves $\bar{\mu}(t)$ and $\bar{T}_{fric}(t)$ of each load case.

### *4.1 Identification of friction model*

To identify a single set of coefficients and exponents associated to Equation (4), which is valid for all load cases, a numerical multi-case optimization task according to [16] is set up considering all 12 averaged brake processes. The input time histories of each load case are the mean curves $\bar{T}_{fric}(t)$ and $\bar{F}_C(t)$ from the measurements. Within the optimization task the simulated friction curves are fitted to $\bar{\mu}(t)$ by tuning the model parameters. The identification results are given in Table 2. It is necessary to point out, that the parameters are representing the investigated pad material applied on a particular wheel-disc brake. Other materials or pad-disc pairings might yield significantly

different values. Figure 9 shows the graphical comparison of the normalized plots of the 12 averaged measurements $\bar{\mu}(t)$ with the simulation results using Equation (4) and the parameters from Table 2. It exposes a good correspondence between simulation and measurement and underlines the individual behavior according to each load case. The four curve shares, each representing one initial velocity, as well as the slight differences for an identical initial velocity due to different mass $m_{eff}$ and clamp force $F_C$ are well represented by the model. In case of brake applications with 100 km/h the COF is mostly increasing, whereas an increasing initial velocity leads to a reduction of friction at the beginning of the brake process. This load case dependent behaviour is correctly captured by the model and explains the characteristics of the deceleration observed in Figure 1 and the decreasing mean values of the averaged COF $\bar{\mu}_s$ shown in Figure 4. The deviations between simulation and measurement at the end of the brake processes are mainly caused by averaging the measured single brake processes, which are not of equal length in time, to one curve. Furthermore, at the end of the brake process stick-slip effects might occur, which are not captured by the model. Since the velocity is approaching zero at the end, these effects are of minor importance for the braking distance. However, to evaluate the applicability of the model within velocities close to zero further investigations are necessary.

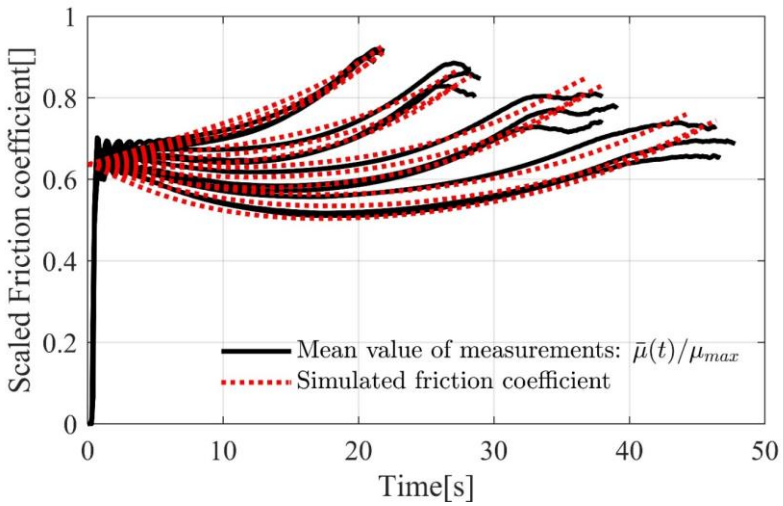


Figure 9: Scaled comparison of simulated COF with mean measured COF for each load case (Curves shares from top to bottom: $v_0$=100,120,140,160 km/h)

Table 2: Identified parameters of friction model

| | | | | |
|---|---|---|---|---|
| Coefficients | $a = 0.008$ | $b = 0.010$ | $c = 0.042$ | $d = 0.036$ |
| Exponents | $x = 0.994$ | $y = 0.533$ | $z = 1.581$ | $r = 0.367$ |

### *4.2 Identification of temperature model*

The procedure described above is applied to identify the thermal disc brake model described by Equations (5)-(10). In this case the input time histories of each load case are the mean curves $\bar{\mu}(t)$ and $\bar{F}_C(t)$ from the measurements. Table 3 specifies the results of the numerical multi-case optimization considering all 12 load cases. As mentioned before, the parameter values correspond to the investigated wheel-disc brake and might vary dependent on configuration of the disc and its material. Figure 10 graphically compares the averaged measurements with the identified thermal model and shows the very good agreement between measurement and simulation.

Table 3: Identified parameters of temperature model

| | | | |
|---|---|---|---|
| Heat capacities | $C_{fric} = 7191\ \frac{J}{K}$ | $C_{disc} = 24156\ \frac{J}{K}$ | |
| Conduction | $G_{ref} = 691\ \frac{W}{K}$ | $\frac{\partial G}{\partial T} = -1.31\ \frac{W}{K^2}$ | |
| Surface Convection | $h_0 = 5\ \frac{W}{Km^2}$ | $h_{ref} = 30\ \frac{W}{Km^2}$ | $ex = 0.4$ |
| Ventilation Convection | $h_0 = 5\ \frac{W}{Km^2}$ | $h_{ref} = 30\ \frac{W}{Km^2}$ | $ex = 0.6$ |

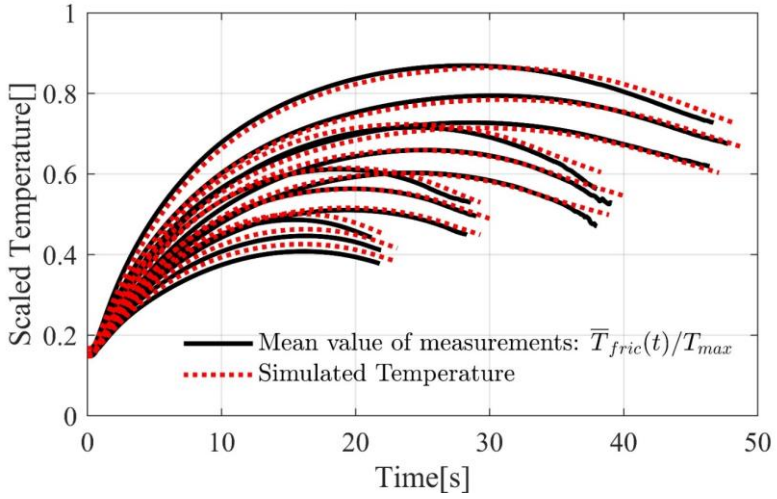


Figure 10: Scaled comparison of simulated averaged surface disc temperature $T_{fric}$ with mean measured averaged surface disc temperature for each load case (Curves shares from top to bottom: $v_0$=160,140,120,100 km/h)

## 5 Stochastic model identification

To extend the deterministic model from Sec. 3 for stochastic influences we apply two working hypotheses:

1. We assume a Gaussian distribution of the phenomena that rule the probability of the COF.

2. The adopted statistical model is based on Equation (4) and considers its coefficients $a, b, c, d$ as well as the initial value of the COF $\mu_0$ to be in general uncertain and subject of random variations.

An indication on the validity of the first hypotheses is given in the exemplary quantile-quantile plot in Figure 11. There, the deviations from the normal distribution are comparatively small. Similar deviations are found for other load cases and other points of time.

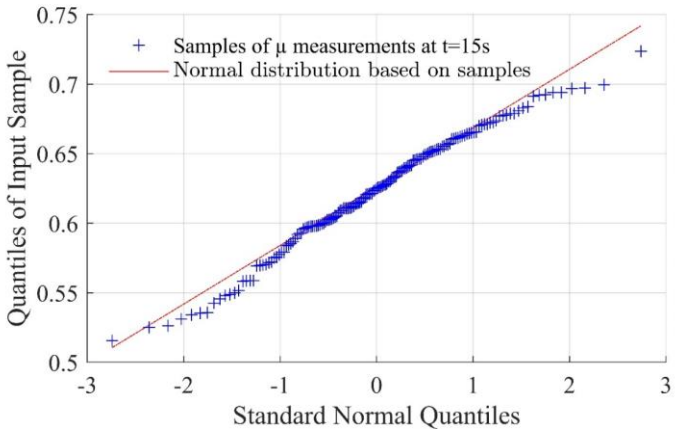


Figure 11: Quantiles of 163 values of the scaled instantaneous COF at t=15s in load case V0140_Case1 (y-axis) versus quantiles of corresponding standard normal distribution (x-axis)

The stochastic identification based on the second hypothesis demands to identify the distributions of the uncertain coefficients that yield the observed stochastic of the COF. Note that this inverse problem appeared to be inconclusive, so several combinations of scatter of the assumed stochastic coefficients $\mathrm{a}, \mathrm{b}, \mathrm{c}, \mathrm{d}$ might yield similar results. It is found that it is sufficient to consider only two uncertain parameters: the initial value $\mu_0$ and the coefficient a.

A multi-case optimization task is set up to fit the friction model to the upper and lower boundaries $\bar{\mu}(t) \pm 3\sigma_\mu(t)$ of the COF by tuning the parameters a and $\mu_0$. The result is an interval for both parameters, which are interpreted as $6 \cdot \sigma_{\mu_0/\mathrm{a}}$ yielding:

$$\begin{aligned} \mu_0 &\sim \mathcal{N}\left(\bar{\mu}_0 = \mu_0,\ \sigma_{\mu_0} = 0.01\right), \\ a &\sim \mathcal{N}\left(\bar{a} = 0.008, \sigma_a = 0.001\right). \end{aligned} \tag{13}$$

Random variations of the temperature model parameters have been neglected, since a major source for the temperature scatter in Figure 6 can be associated to spatial temperature distribution on the disc surface, which is assumed to have a minor influence

on the COF. To validate the resulting stochastic friction model based on the identified sensitive parameters and their distribution, a Monte-Carlo Simulation (MCS) of the dynamometer model shown in Figure 8 is performed. Within a MCS a large number of numerical simulations is performed based on artificially generated random inputs or parameters to analyze the propagation of uncertainty on the output. In this case 200 simulations for each load case were performed. The parameters $a$ and $\mu_0$ take a new value for each single simulation according to their distribution given in Equation (13).

Figure 13 presents the plots of the instantaneous mean of the COF measurements $\bar{\mu}(t)$ versus the MCS for all 12 load cases including the domain limited by three times the instantaneous standard deviations $\sigma_\mu(t)$. Figure 12 compares the resulting mean values of the averaged COF over distance $\bar{\mu}_s$ and their standard deviation $\sigma_{\mu_s}$ with the ones estimated from the measurements. Both figures show that the stochastic friction model represents the measured instantaneous and averaged stochastics quite well. Smaller deviations of the variance occur for the second and third load case of 100 km/h and the first load cases of 140 km/h and 160 km/h, which indicates that there are still minor stochastic processes that are not yet covered by the model. Nevertheless, the overall results are satisfactory and it is concluded that it is sufficient to consider a stochastic friction model based on two uncertain parameters linked to a deterministic temperature model to capture the uncertainty of the COF.

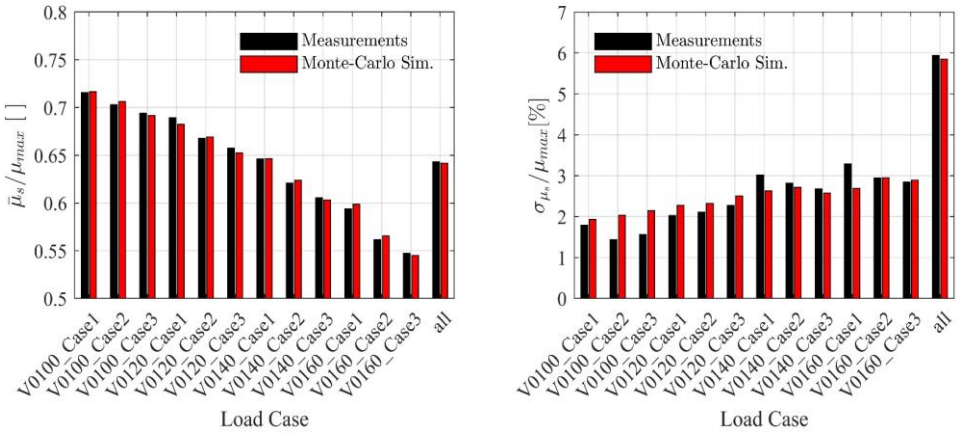


Figure 12: Comparison of scaled mean values (left) and empirical standard deviation (right) of measured and simulated averaged COFs over distance for each load case

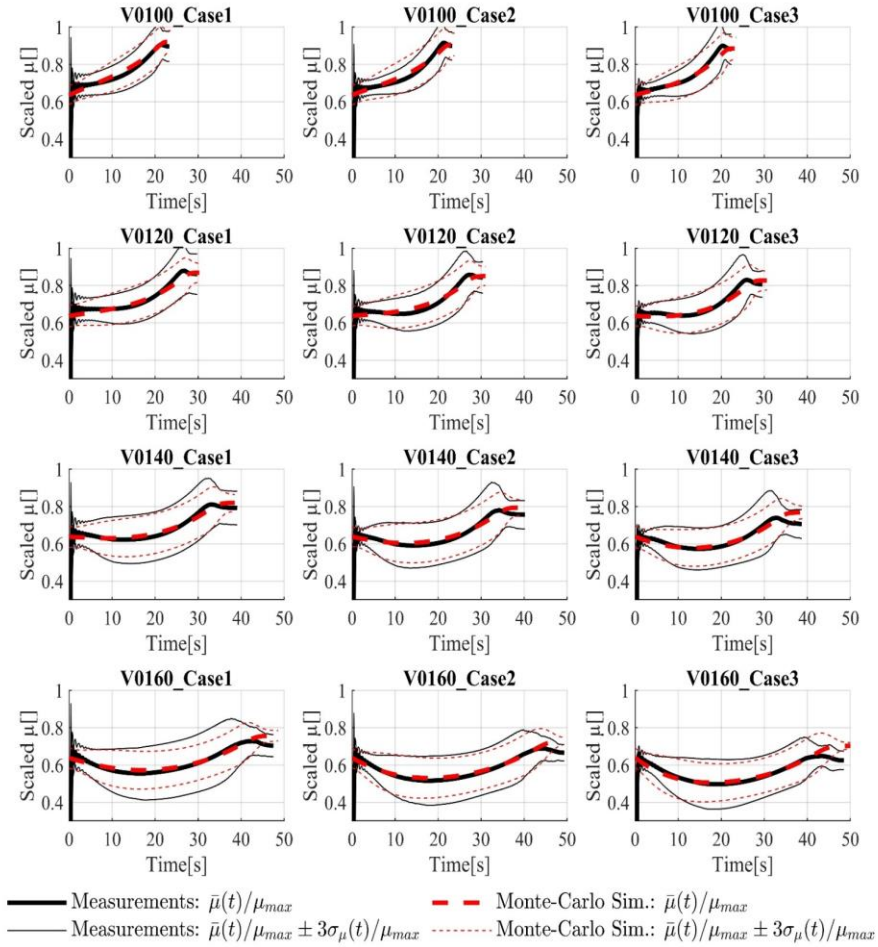


Figure 13: Scaled comparison of instantaneous mean value of COF and empirical standard deviation of measurements and MCS with 200 simulations for each load case

## 6 Simulation of field test

### *6.1 Field test measurements*

In this section the modelling knowledge gained by the analysis of the dynamometer test rig results is transferred to field tests. For this purpose, measurements of a multiple unit train set carried out on a test circuit are used. The vehicle is assembled of four bogies and a total of eight axles with two brake units each. Table 4 presents the scenarios that have been performed using friction brakes only, i.e. without application of the electrodynamical brakes. The same type of brake pad but different specimens as in the dynamometer test rig were used and two different sets were mounted alternatively. All brake applications were performed under dry rail and pad conditions.

Table 4: Number of friction brake applications performed with train according to load case, pad and actuation types (effective mass and clamp forces are mean values over all brake units, EP=electro-pneumatic actuation, PN=indirect-pneumatic actuation)

| Load case | | | | Pad Set | Actuation Type | Number of brake applications per initial velocity $v_0$ | | | | |
|---|---|---|---|---|---|---|---|---|---|---|
| Brake Mode | Load | $\bar{m}_{eff}$ $[kg]$ | $\bar{F}_C$ $[kN]$ | | | $v_0 = 100$ $[km/h]$ | $v_0 = 120$ $[km/h]$ | $v_0 = 140$ $[km/h]$ | $v_0 = 160$ $[km/h]$ | Σ |
| emergency | empty | 7574 | 36 | Set 1 | EP | 1 | 3 | 0 | 1 | 5 |
| | | | | | PN | 1 | 4 | 1 | 1 | 7 |
| | | | | Set 2 | EP | 1 | 4 | 1 | 1 | 7 |
| | | | | | PN | 1 | 1 | 1 | 1 | 4 |
| | normal | 8993 | 44 | Set 1 | EP | 1 | 5 | 1 | 1 | 8 |
| | | | | | PN | 2 | 3 | 1 | 2 | 8 |
| | max. | 9292 | 45 | Set 2 | EP | 2 | 4 | 1 | 1 | 8 |
| | | | | | PN | 1 | 1 | 1 | 1 | 4 |
| service | empty | 7574 | 33 | Set 1 | EP | 2 | 4 | 1 | 2 | 9 |
| | | | | Set 2 | EP | 1 | 5 | 1 | 1 | 8 |
| | normal | 8993 | 36 | Set 1 | EP | 1 | 7 | 1 | 1 | 10 |
| | | | | Set 2 | EP | 2 | 6 | 1 | 1 | 10 |
| All load cases, pad sets and actuation types | | | | | | **16** | **47** | **11** | **14** | **88** |

The running resistance of the train set has been investigated in run-out experiments, so that the resistance formula

$$F_R\big(v(t)\big) = \mathrm{A} + \mathrm{B} \cdot v(t) + \mathrm{C} \cdot v(t)^2 \tag{14}$$

could be parametrized and exploited to consider its influence on the measurements. In addition, the weight of the train set has been measured, so that each load is quantified correctly. The given transient measurements include the pneumatic pressure $p_c(t)$ at each axle, one deceleration $d(t)$ and one velocity $v(t)$ for the entire vehicle and the temperature $T_{fric}(t)$, represented by a single measurement point at the surface of one of the 16 disc brakes.

### *6.2 Deterministic and stochastic field test simulations*

Figure 14 displays the basic set-up of the simulation model implemented in *Dymola*® based on the physical modeling language *Modelica*®. The vehicle is a single mass initialized with the initial velocity $v_0$ from the train measurements, which is decelerated by the running resistance and 16 individual brake torques actuated by 16 measured pneumatic pressure values $p_c(t)$. The brake torques are simulated using the above presented friction and temperature model, which is adapted to consider a larger disc diameter compared to the dynamometer tests. It is initialized with the temperature $T_0$, which is the start value gained from the temperature measurements. The friction

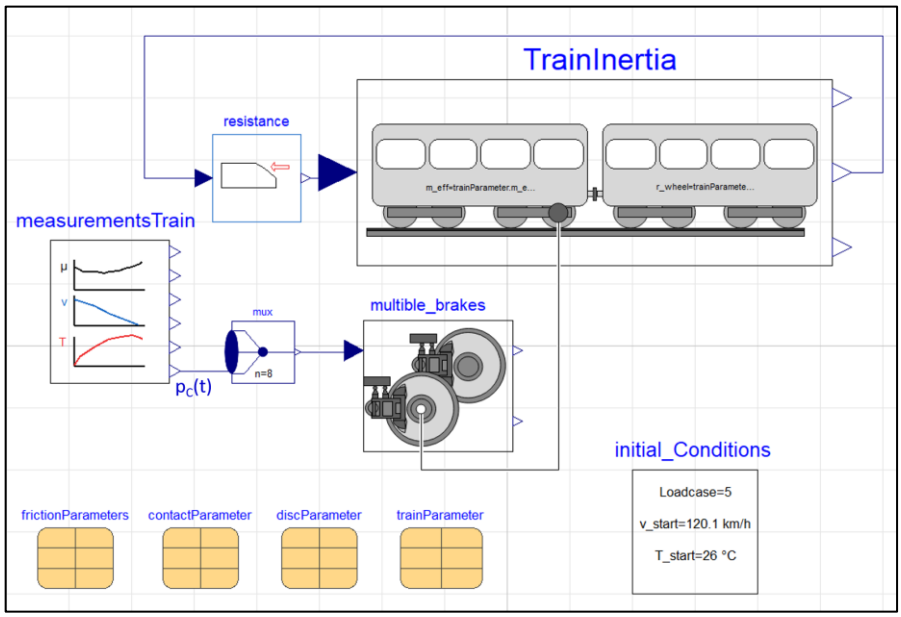


Figure 14: Basic set-up of simulation model in Dymola®

velocity $v_{fric}(t)$ depends on the given wheel and friction radii and the simulated vehicle velocity $v(t)$, while perfect rolling is assumed, since no macroscopic slip is noticed in the measurements.

Three different simulation set-ups are defined (DS=deterministic simulation, MCS =Monte-Carlo simulation):

- **DS**: The simulations do not assume any stochastics, but only take the purely deterministic model from Sec. 3 and Sec. 4 into account.
- **MCS-100**: Each of the 88 brake processes from Table 4 is simulated 50-times with stochastically varied parameter values according to Sec. 5, while it is assumed that all parameters scatter independently from each other:

  $a_{ij} \sim \mathcal{N}(\bar{a} = 0{,}008,\ \sigma_a = 0{,}001)$ , $\mu_{0ij} \sim \mathcal{N}(\bar{\mu}_0 = \mu_0,\ \sigma_{\mu_0} = 0{,}01)$,

  where index $i$ denotes each simulation and $j$ indicates each brake disc. Hence, a MCS with all together $50 \cdot 88 = 4400$ individual representations is performed. In addition, the running resistance varies with $A_i \sim \mathcal{N}(\bar{A} = 2500,\ \sigma_A = 1600)$, which is derived from the deceleration data at the beginning of each brake process. The variations of the brake pressure values are contained in the measurements $p_c(t)$. Other variations, such as the caliper parameters, are assumed to be irrelevant since all components were quite new and belong to a single vehicle.
- **MCS-75/25**: This set-up corresponds to MCS-100, except to the friction model, where a 75% global variation that is identical for all 16 brake discs and a 25% individual scatter are presumed, i.e.:

  $a_i \sim \mathcal{N}(\bar{a} = 0{,}008,\ \sigma_a = 0.75 \cdot 0{,}001)$, $a_{ij} \sim \mathcal{N}(\bar{a} = a_i,\ \sigma_a = 0.25 \cdot 0{,}001)$,

  $\mu_{0i} \sim \mathcal{N}\left(\bar{\mu}_0 = \mu_0,\ \sigma_{\mu_0} = 0.75 \cdot 0{,}01\right)$, $\mu_{0ij} \sim \mathcal{N}(\bar{\mu}_0 = \mu_{0i},\ \sigma_{\mu_0} = 0.25 \cdot 0{,}01)$.

  The idea of this approach originates from two UIC documents [17] and [18],

where 67% and 33% or 75% and 25% partitions, respectively for global and individual scatter are chosen and motivated by experiences in practice.

### *6.3 Presentation and discussion of results*

With the available set of data, it is not possible to measure the COF acting in each single brake unit of the railway vehicle or estimate this parameter for single axles or bogies using a state observer, as proposed in [19]. However, it is possible to estimate the *effective* COF $\mu_{eff}$, representing the frictional behavior of all acting brake units by a single coefficient, to analyze the deterministic and stochastic frictional behavior of the brake pads during field test. It is calculated by relating the braking forces minus the resistance forces $F_R$ and the sum of all clamp forces $F_{C_i}$, scaled by friction and wheel radii:

$$\mu_{eff}(t) = \frac{\mathrm{m_{eff}} \cdot d(t) - F_R(v(t))}{\sum_{i=1}^{16} \frac{\mathrm{r_{fric_i}}}{\mathrm{r_{wheel_i}}} \cdot F_{C_i}(t)} \tag{15}$$

Figure 15 compares the measurements with the results of the three simulation set-ups with respect to the averaged *effective* COF $\mu_{s,eff}$ calculated according to Equation (15) and Equation (3). The mean value $\bar{\mu}_{s,eff}$ is in general met with all three simulation set-ups. Very good accordance between measurement and simulations is visible for $v_0$ =120 km/h and $v_0$ =140 km/h, whereas smaller deviations occur for initial velocities of 100 km/h and 160 km/h. For both field test and simulation, a reduction of the mean value is observed for an increasing initial velocity, whereas the variance tends to grow. In case of both pad sets applied in the field test the mean values of the simulations are, however, subject to a slightly higher gradient. The systematic difference of the mean values is the root cause of the larger variance observed for the simulation models compared to the measurements, if all initial velocities are considered

at once. Assuming the simulation results correctly represent the pads analyzed on the test rig, the reason for the deviation of the mean values could be a different frictional behavior of the specimen analyzed on the test rig in comparison to the pad sets applied in the vehicle, e.g. due to different batches.

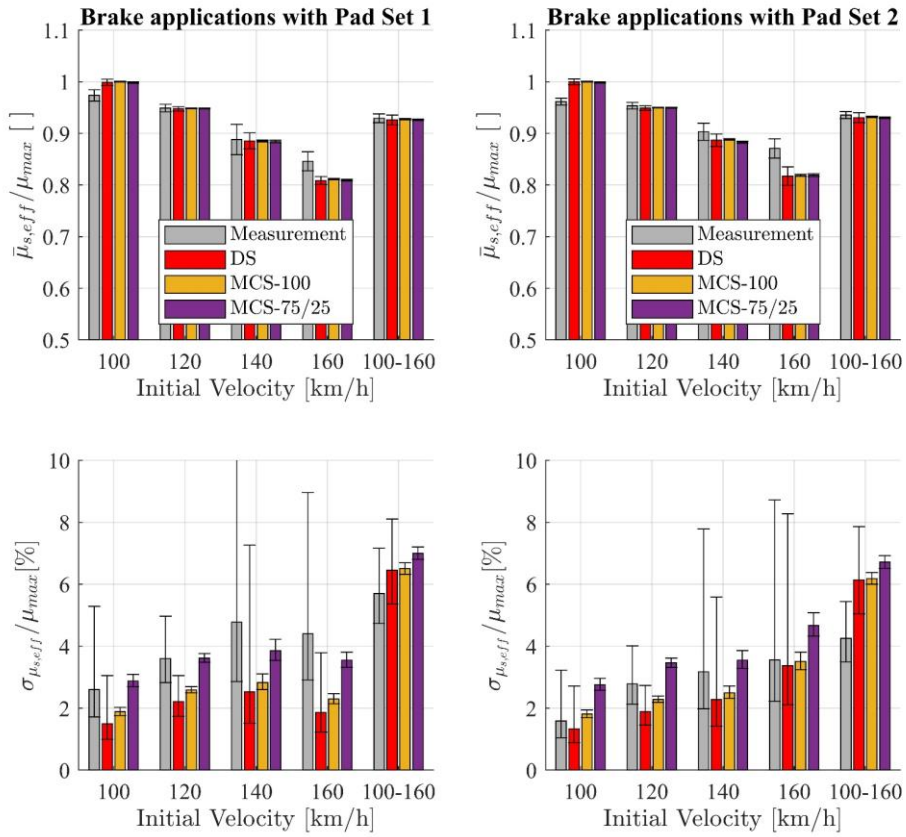


Figure 15:Mean value (upper graphs) and relative standard deviation (lower graphs) of effective COF averaged over braking distance from measured and simulated brake applications for all load cases of Pad Set 1(left graphs) and Pad Set 2 (right graphs) with respect to initial velocity. Error bars represent 95% confidence intervals calculated for mean values based on a T-distribution and calculated for standard deviation based on a $\chi$2-distribution.

Since a good accordance between measured and simulated disc temperatures is found, the influence of different ambient conditions on the test rig and in the field is excluded as root cause for the systematic difference of $\bar{\mu}_{s,eff}$ between field test and

simulation. Furthermore, errors of the simulated resistance force have been shown to be small. Considering these observations, it is concluded that the main cause for the slight differences of $\bar{\mu}_{s,eff}$ is caused by different frictional characteristics of the specimen on test rig and on the vehicle, although the same pad material is used. This result points out that the presented model-based extrapolation from test rig to field tests might be prawn to errors, if the pads or batches applied in the vehicle significantly differ from the ones analyzed on the test rig.

The comparison of the MCS (yellow and purple bars) and the deterministic simulation (red bar) verify that the mean values of the stochastic friction models represent the deterministic model, as requested. This result is to be expected because the deterministic model is tailored to represent the mean values. Note that the scatter yielded by the deterministic simulations (red bars of $\sigma_{\mu_{s,eff}}$,) stems from varying load cases consolidated for one initial velocity, i.e. load, brake mode and actuation types shown in Table 4. In addition, slightly varying simulation inputs and initial conditions $F_C$, $T_{fric,0}$ and $v_0$ are responsible for the scatter of the deterministic simulations despite identical load cases.

Analysing the standard deviations $\sigma_{\mu_{s,eff}}$ in Figure 15, it becomes apparent, that the individual variance of each brake disc, simulated by **MCS-100**, is only leading to a small extension of the variance compared to the deterministic variance (compare yellow and red bars of $\sigma_{\mu_{s,eff}}$). This seems reasonable, since $\mu_{s,eff}$ is becoming the mean value of the single $\mu_{s,i}$ acting in all brake discs of the vehicle, if the clamp forces and radii are assumed to be equal for each disc. Therefore, an *independent* scatter of each friction value is scaled by the number of brake units $n$ according to the law of large numbers $\sigma_{\mu_{s,eff}} \approx \frac{\sigma_{\mu_s}}{\sqrt{\mathrm{n}}}$. It can be followed that the influence of the individual scatter of each brake

disc on the scatter of the deceleration of the train is decreasing with an increasing number of brake discs, i.e. longer train sets, as also shown in [20].

However, the comparison of the measured and simulated relative standard deviation shows that the assumption of a correlation between the frictional behavior of the single brake discs for a single simulation, simulated by **MCS-75/25** (compare grey and purple bars of $\sigma_{\mu_{s,eff}}$), is yielding good accordance with the variance of the measurements, in particular for pad set 1. A possible cause for the correlation of the frictional behaviour of the single brake discs is the similar load history that all pads applied in the same vehicle have in common. According to observations described in [21], the structure of the frictional boundary layer is driven by the mechanical and thermal loads that it was exposed to. If the same brake applications are performed multiple times a certain structure is established in the boundary layer, which is modified as soon as the external loads are changing, i.e. different brake applications are conducted. This grind-in effect leads to similar pad surfaces of all brake discs with similar load histories, which in turn might result in a correlation of the COF of all brake pads. Furthermore, this theory implies that the scatter between different brake applications, which affects all brake pads of a single train to the same extent, is driven by the dimension of the variances of the individual load cases. If a train serially performs identical brake applications, the scatter of the deceleration between the single brake applications is thus presumably reduced to a particular value. These observations suggest to consider the expected variance of the load history when estimating the scatter of the deceleration due to frictional brake torques. In order to transfer this behaviour to the stochastic model approach presented in this work, the parameter variation considered in the MCS needs to be coupled to the previous load cases. This approach is, however, subject for future work.

Figure 16 compares the mean value and the empirical standard deviation of simulated and measured braking distances of different load cases with the velocity $v_0 = 120\ \mathrm{km/h}$ and each pad set. The selected load cases specified by load (empty, normal, max), brake mode (emergency, service) and actuation type (EP, PN) correspond to brake applications that were performed at least 4 times during field test (see Table 4). Since the number of brake applications of identical load cases is limited, the nominal braking distance cannot be properly estimated for other initial velocities due to the uncertainty of the measurements. Note, the scatter of the braking distance for the deterministic model is mainly caused by small deviations of the initial velocity from

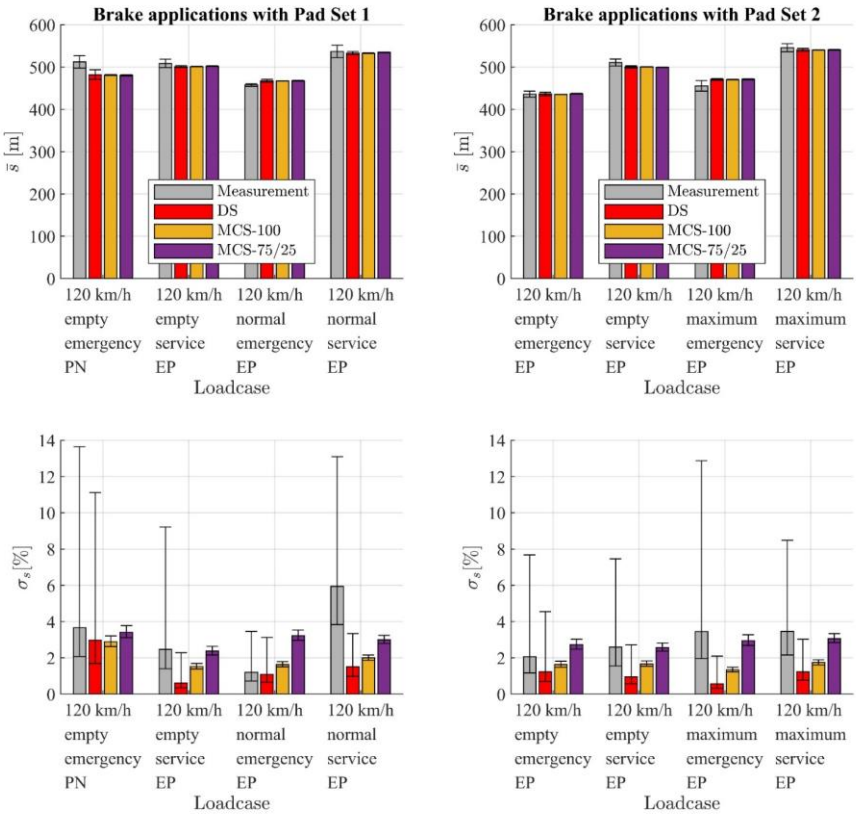


Figure 16: Mean value (upper graphs) and relative standard deviation (lower graphs) of braking distance estimated from measured and simulated load cases with 120 km/h specified by load, brake mode and actuation type of Pad Set 1(left graphs) and Pad Set 2 (right graphs). Error bars represent 95% confidence intervals calculated for mean values based on a T-distribution and calculated for standard deviation based on a $\chi 2$-distribution.

120 km/h. The braking distance is not corrected to visualize this effect.

The mean values represent the nominal braking distance $\bar{s}$ of the selected load cases. The mean relative differences of $\bar{s}$ between deterministic simulation and measurement are 2,6% for pad set 1 and 1,6% for pad set 2, the maximum relative differences are 5,8% for pad set 1 and 3,4% for pad set 2, respectively. Hence, the simulation provides a more accurate estimation for the nominal braking distance of these load cases if pad set 2 is mounted. This result suggests that the brake pads of set 1 and set 2 do systematically differ from each other and underlines the influence of the individual behavior of the specimen or underlying material batches on the estimation of the braking distance. It is important to mention that the load cases presented in Figure 16 are not identical (compare load, actuation type and brake mode of pad set 1 and 2), which could also be a cause for the different accuracy of the model, e.g. due to slight deviations of the real and simulated mass of the train.

The uncertainty of the measured braking distance is quantified by the confidence intervals in Figure 16. For most of the selected load cases the confidence intervals of measured and simulated mean values $\bar{s}$ overlap, which underlines the satisfying accuracy of the simulations. In addition, the interval size highlights how the enlargement of realizations, i.e. brake applications artificially performed in the MCS, is reducing the estimation uncertainty (50 simulations for each measured brake application), especially for the variance of the braking distance. In case of the second load case for pad set 1 (120 km/h, empty, service, EP) the estimated relative standard deviation of the measured braking distance might take values from $1\sigma_s \approx 2 - 9\%$, although the scatter due to the initial velocity is quite small. It is obvious that these uncertainties are caused by limited capabilities during field testing (n=4, as shown in Table 4).

The point estimation of the relative standard deviation $\sigma_s$ yields values between $1\sigma_s = 1\%$ to 6% for the measured braking distance including the scatter of the initial velocity. As the comparison of the deterministic model and the measurements reveals (compare grey and red bars of $\sigma_s$), a non-negligible proportion must be caused by the scatter of the deceleration. For most of the load cases of both pad sets the braking distance scatter is in good accordance with the estimation based on the MCS with correlated friction behavior (**MCS 75/25**), whereas the scatter from **MCS 100** is mostly to small. The mean difference between estimated standard deviation based on **MCS 75/25** and the estimation based on the measurements is 1,33% for pad set 1 and 0,40% for pad set 2. These results confirm the previous results regarding the scatter of the averaged COF and underline that the ratio of correlation between all brake pads of a vehicle is a sensitive parameter regarding the correct estimation of the braking distance variance.

## 7 Conclusions and outlook

In this work the deterministic and stochastic behavior of the coefficient of friction (COF) of brake pads applied for disc brakes in railway vehicles has been analyzed and modelled. The analyzation of the measurement data recorded on a full-scale dynamometer test rig reveals the strong load case dependency of both, COF and surface temperature. This observation motivates the application of mathematical models to predict this individual behavior. The friction and temperature models presented in this work demonstrate that it is possible to simulate the observed behavior based on a single set of parameters identified with numerical optimization. Moreover, this work proposes an inverse identification procedure to map the immanent stochastic nature of the COF based on Monte-Carlo Simulation (MCS). It is shown that the consideration of two

uncertain parameters of the friction model is sufficient to satisfactorily simulate the variance of the COF. Applying the models for the simulation of field tests of an entire train yields good accordance with measurements. Smaller deviations are presumably caused by different frictional characteristics of the specimen on the test rig and the ones applied on the vehicle. This points out that systematic differences between specimen identified on the test rig and the ones applied in field test, e.g. due to different batches, might affect the accuracy of the model. A mean relative deviation of the estimated nominal braking distance between measurements and simulations smaller than 3% and a maximum deviation smaller than 6% was observed for 120 km/h. Finally, MCSs of the train brake applications suggest that the stochastics of all brake pads applied in the same railway vehicle correlate during a single brake application.

The results reveal the potential of numerical simulations for railway brake applications and suggest to use more elaborate specifications of the COF to predict the nominal braking distance according to [2, 3] and probability distribution of the averaged deceleration according to [18]. Thus, time-consuming and costly experiments can be enriched by a large number of virtual tests to improve the estimation of the system behavior and to shorten approval procedures. This includes the analysis of entire vehicle dynamics during braking, as presented in [22].

The identification and verification of the models in this work was performed for good adhesion conditions, i.e. dry rails and pads. To extend the usability of the presented models, they need to be investigated regarding bad conditions of both, pads and rail. Besides modelling the influence of moisture on the pad performance, which may be analyzed by test-rig data, the influence of the wheel-slide protection system on the prediction of the brake performance needs to be investigated. Furthermore, the identification and verification process does not yet include the influence of wear during

service, which affects the performance of pads and temperature evolution in the brake components. The aforementioned investigations require to couple the findings of this work with modelling approaches to estimate wear and the adhesion acting in wheel-rail interface.

Finally, the results need to be assessed and confirmed by applying and refining models and methods for other pad materials, disc types and data bases. This includes the detailed assessment of the reliability regarding the prediction of the braking distance in terms of uncertainty quantifications and the comparison to conventional methods in order to establish confidence in the industrial sector as well as standardization and assessment bodies.

## Acknowledgements

This work is partly sponsored by Knorr Bremse SfS GmbH. The authors would like to thank all colleagues from Knorr-Bremse for their support during the common project. This includes the exchange of expertise and the provision of measurement data, which is indispensable for this work.

## References

[1] European-Comission, Commission Regulation (EU) No 1302/2014 of 18 November 2014 concerning a technical specification for interoperability relating to the 'rolling stock — locomotives and passenger rolling stock' subsystem of the rail system in the European Union, 2014.

[2] E. 14531-1:2005, Railway applications –Methods for calculation of stopping and slowing distances and immobilisation braking – Part 1: General algorithms utilizing mean value calculation for trainsets or single vehicles, 2019.

[3] EN-14531-2: 2016-04, Railway applications –Methods for calculation of stopping and slowing distances and immobilisation braking – Part 2: Step by step calculations for train sets or single vehicles, 2016.

[4] Ehret M, Identification of a dynamic friction model for railway disc brakes. Proceedings of the Institution of Mechanical Engineers, Part F: Journal of Rail and Rapid Transit. 2021.

[5] Lee NJ and Kang CG, The Effect of a Variable Disc Pad Friction Coefficient for the Mechanical Brake System of a Railway Vehicle. PLoS ONE. 2015; 10(8).

[6] EN-15328: 2020-10, Railway applications - Braking - Brake pads. 2020.

[7] Ostermeyer G, On the dynamics of the friction coefficient. Wear. 2003; 254(9): 852-858.

[8] Wasilewski P, Frictional Heating in Railway Brakes: A Review of Numerical Models. Archives of Computational Methods in Engineering. 2020; vol. 27: 45-58.

[9] UIC-Code 548: Brakes - Requirements of friction test benches for the international certification of brake pads and brake blocks. 2016

[10] Dufrénoy P and Weichert D, Prediction of railway disc brake temperatures taking the bearing surface variations into account, Proceedings of the Institution of Mechanical Engineers, Part F: Journal of Rail and Rapid Transit. 1995; 209: 67-76.

[11] Gigan GL, Vernersson T, Lunden R , et al. Disc brakes for heavy vehicles: an experimental study of temperatures and cracks. Proceedings of the Institution of Mechanical Engineer,s Part D: Journal of Automobile Engineering. 2015; 229: 684-707.

[12] Ricciardi V, Augsburg K, Gramstat S, et al. Survey on Modelling and Techniques for Friction Estimation in Automotive Brakes. Applied Science. 2017; 7(9).

[13] Limpert R, Brake design and safety. Warrendale. PA. USA. SAE International. 2011.

[14] Sheridan DC, Kutchey JA, Samie F, Approaches to the thermal modeling of disc brakes. SAE Transactions, 1988; 268-283,.

[15] G. P. Voller, Analysis of heat dissipation from railway and automotive friction brakes, Brunel University, 2003.

[16] Pfeiffer A., Optimization Library for Interactive Multi-Criteria Optimization Tasks. In Proceedings of 9th International Modelica Conference. 2012; 669-679.

[17] International Union of Railways, UIC B126/DT421: Comparison between probabilisteic mathematical safety margins calculations and operation data. 2008.

[18] International Union of Railways, UIC B126/DT414: Braking questions: Methodology for the safety margin calculation of the emergency brake intervention curve for trains operated by ETCS/ERTMS. 2006.

[19] Schwarz C, Lüdicke D, Heckmann B, Friction Estimation for Railway Brake Systems in Field Tests. Proceedings of the International Railway Symposium Aachen 2019: 608-623.

[20] Jeanichen D and Krönert T, Der stochastische Anhalteweg bei Schnellbremsung unter Beachtung der Anzahl der Fahrzeuge des Zuges. Eisenbahntechnische Rundschau. 2017; 3 48-53.

[21] Ostermeyer GP and Wikening L, Experimental Investigation of the Topology Dynamics in Brake Pads. SAE International Journal of Passenger Cars-Mechanical Systems. 2013; 6: 1398-1407.

[22] Heckmann A, Ehret M, Gether G, et al. Overview of the DLR RailwayDynamics Library. Proceedings of the 13th international Modelica Conference. 2019; 157: 323-332.